ISSN 1070-3284, Russian Journal of Coordination Chemistry, 2021, Vol. 47, No. 1, pp. 81–87. © Pleiades Publishing, Ltd., 2021.

Crystal Structure of $[Pd(Imt)_4]Cl_2$ and DFT Studies of $[Pd(Imt)_4]Cl_2$ and $[Pd(Imt)_2(CN)_2]$ (Imt = Imidazolidine-2-Thione)

H. Sadaf[a], W. Zierkiewicz[b], M. Michalczyk[b], S. Ahmad[c, *], Imtiaz-ud-Din[a], M. Nawaz Tahir[d], A. A. Isab[e], A. R. Al-Arfaj[e], and S. Nadeem[a]

[a]*Department of Chemistry, Quaid-i-Azam University, Islamabad, Pakistan*

[b]*Department of Chemistry, Wroclaw University of Technology, Wroclaw, 50-370 Poland*

[c]*Department of Chemistry, College of Sciences and Humanities, Prince Sattam bin Abdulaziz University, Al-Kharj, 11942 Saudi Arabia*

[d]*Department of Physics, University of Sargodha, Sargodha, Pakistan*

[e]*Department of Chemistry, King Fahd University of Petroleum and Minerals, Dhahran, 31261 Saudi Arabia*

**e-mail: saeed_a786@hotmail.com*

Received February 14, 2020; revised April 13, 2020; accepted April 17, 2020

Abstract—The crystal structure of a palladium(II) complex of imidazolidine-2-thione (Imt), $[Pd(Imt)_4]Cl_2$ (**I**) was determined by X-ray crystallography (CIF file CCDC no. 1946290). The structure of complex **I** is ionic consisting of $[Pd(Imt)_4]^{2+}$ cation and two chloride counter ions. The palladium atom in the complex ion assumes a distorted square planar geometry. The complex cation and non-coordinated chloride ions are connected to each other through electrostatic and hydrogen bonding interactions. To compare the stability of **I** with its corresponding non-ionic species $[Pd(Imt)_2Cl_2] \cdot 2Imt$ (**Ia**), DFT calculations were performed in the gas phase as well as in the DMSO solvent. The IR spectra of the ligand Imt and complex **I** were reliably interpreted theoretically. The structures of two related cyanide complexes; $[Pd(Imt)_2(CN)_2]_2$ (**II**) and $[Pd(Imt)_4][Pd(CN)_4]$ (**IIa**) were also predicted by DFT calculations in terms of geometries and stability. The DFT results reveal that in the gas phase, the structure **I** is less stable in comparison to the calculated structure **Ia** by 11.26 kcal/mol (ΔG) but reverse is true when the DMSO solvent is included in the quantum chemical calculations. For the cyanide analogues, the ionic dinuclear form **IIa** is more stable than the dimer **II** of the mononuclear complex $[Pd(Imt)_2(CN)_2]$ in gas phase by 13.37 kcal/mol but is less stable in calculations with DMSO by 6.86 kcal/mol.

Keywords: palladium(II) complexes, imidazolidine-2-thione, cyanide, crystal structure, DFT calculations

DOI: 10.1134/S107032842101005X

INTRODUCTION

Palladium(II) complexes of thiones have received considerable attention because of their promising antibacterial and antitumor activities [1–3]. They are also important for catalytic applications particularly in the C–C bond formation [4, 5]. The structural studies on binary palladium(II) complexes of thiones with various anions reveal that these complexes usually exist in the ionic form as $[Pd(thione)_4]X_2$ [6–13]. A few non-ionic and dinuclear complexes are also known [4]. The palladium(II) ion in these complexes exhibits a square planar geometry. Some reports on the crystal structures of palladium(II) complexes of imidazolidine-2-thione (Imt) are also available in the literature [14, 15], which describe that Imt binds as a neutral and terminal S-bonded ligand. On the other hand, the analogous ligands with aromatic skeleton for example, 2-mercaptopyridine may coordinate in neutral as well as anionic form [2, 16]. Our interest in palladium(II) compounds bearing thiourea type ligands is based on preparation of new biologically active species and to explore their structural aspects [3, 6, 7, 17–20]. In view of this interest, the present work describes the structural characterization and DFT analysis of a palladium(II) complex of imidazolidine-2-thione (Imt), $[Pd(Imt)_4]Cl_2$ (**I**). DFT calculations were performed to get the structural insights in the gas phase as well as in solution form and to compare the stability of **I** with the corresponding non-ionic species, $[Pd(Imt)_2Cl_2]\cdot 2Imt$ (**Ia**). The structures of the analogous cyanide complexes, $[Pd(Imt)_2(CN)_2]_2$ (**II**) and its ionic form ($[Pd(Imt)_4][Pd(CN)_4]$) (**IIa**), were also analyzed theoretically. The spectral characterization of **I** has been described earlier [17] but the suitable crystals were not obtained in that study. We have previously reported the DFT studies of three $Pd(CN)_2$ complexes of thioureas to get the structural insights and to check the existence of possible non-ionic

($[Pd(L)_2(CN)_2]$) and ionic ($[Pd(L)_4][Pd(CN)_4]$) species [19].

EXPERIMENTAL

Materials and methods. Palladium(II) chloride was purchased from Degussa AG 40474, Dusseldorf, Germany. Potassium tetrachloridopalladate(II) and imidazolidine-2-thione (Imt) were prepared according to the published procedures [6, 21]. The IR spectra were recorded on a Bruker FTIR spectrophotometer using Diamond ATR accessories over the range 4000–400 cm^{-1} with the resolution of 2 cm^{-1}. The ^1H and $^{13}C\{^1H\}$ NMR spectra in DMSO-d_6 were obtained on a Jeol JNM-LA 500 NMR spectrometer operating at frequencies of 500.00 and 125.65 MHz, respectively, at 297 K. The ^{13}C chemical shifts were measured relative to TMS.

Synthesis of complex I. Complex **I** was obtained by adding 0.105 g (1 mmol) Imt in 15 mL methanol–acetonitrile mixture to a solution of 0.165 g (0.5 mmol) $K_2[PdCl_4]$ in 10 mL water. Mixing resulted in the formation of a yellow clear solution. The yield was 66%.

The cyanide complex **II** was prepared as described previously [19]. Its synthesis by a different procedure has also been reported [22].

For $C_{12}H_{24}N_8S_4Cl_2Pd$ (**I**)				
Anal. calcd., %	C, 24.60	H, 4.13	N, 19.12	S, 21.80
Found, %	C, 24.38	H, 4.34	N, 18.73	S, 21.32
For $C_8H_{12}N_6S_2Pd$ (**II**)				
Anal. calcd., %	C, 26.60	H, 3.31	N, 23.17	S, 17.68
Found, %	C, 26.90	H, 3.52	N, 22.93	S, 17.24

X-ray structure determination. Single crystal data collection for complex **I** was performed at 296 K on a Bruker Kappa APEXII CCD diffractometer equipped with a four-circle goniometer and using MoK_α graphite mono-chromated radiation. Structure solution, refinement and all further calculations were carried out using SHELXS/l-2014 [23, 24]. Molecular graphics were performed using PLATON [25]. The crystallographic data and refinement details are presented in Table 1. Selected bond distances and angles are given in Table 2. Hydrogen bond parameters for **I** are listed in Table 3.

Supplementary material for structure **I** has been deposited with the Cambridge Crystallographic Data Centre (CCDC no. 1946290; deposit@ccdc. cam. ac.uk or http://www.ccdc.cam.ac.uk/data_request/cif).

DFT calculations. DFT investigations were carried out for four complexes; $[Pd(Imt)_4]Cl_2$ (**I**), its non-ionic form $[Pd(Imt)_2Cl_2] \cdot 2Imt$ (**Ia**) and two model compounds, $[Pd(Imt)_2(CN)_2]_2$ (**II**) and $[Pd(Imt)_4][Pd(CN)_4]$ (**IIa**) as well as Imt ligand. The calculations at the B3LYP-D3/d95v** [26–28] (hybrid density functional with D3 damping function to include dispersion) level of theory were performed in the gas phase and in DMSO solvent using polarizable continuum model (PCM) [29, 30]. For Pd, S and Cl atoms, LanL2DZ [31] pseudopotentials were utilized in conjunction with d95v** basis set [32]. The initial geometries for optimization were taken from the original crystallographic data of **I** without further restriction during optimization procedure. For all optimization tasks the vibrational frequencies were calculated to ensure that obtained geometries were true minima (no imaginary frequencies). The entities studied are closed-shell systems in which the ground electronic state is singlet. Natural Bond Orbitals (NBO) calculations (GenNBO 5.0 software) were performed to obtain natural atomic charges and visualize HOMO–LUMO orbitals at the 0.05 electron density isosurface [33]. All the computations were carried out by using the Gaussian16 code (Rev. B.01) [34].

RESULTS AND DISCUSSION

The reactions of $K_2[PdCl_4]$ with Imt in a 1 : 2 molar ratio resulted in formation of the desired product $[Pd(Imt)_4]Cl_2$ (**I**). The crystal structure of compound **I** along with the atom labeling scheme is shown in Fig. 1. Compound **I** is ionic consisting of $[Pd(Imt)_4]^{2+}$ complex and two Cl^- ions. The Pd(II) atom in the complex ion is located at inversion center. It is bound to four sulfur atoms of imidazolidine-2-thione ligands in a somewhat distorted square planar geometry. The *cis* angles around Pd are close to 90°, whereas the *trans* angles are 180°. Imt ligands coordinate through sulfur in a monodentate fashion. The Pd–S bond lengths (Table 2) fall within a usual range reported for other four-coordinate palladium(II) complexes of thiones [6–13, (35, 36)]. The two Pd–S bond lengths are nearly the same (2.3362 and 2.3610 Å). The shorter N–C(S) bonds compared to N–C(C) ones indicate the presence of a marked double-bond character in the N–C(S) bond. The C=S bond distance of 1.710 Å is similar to that found for other Imt complexes [14, 37–39]. The angles of $S(1)C(2)N_2$ moiety of the Imt ligand indicate a distortion from the trigonal planar environment. The complex is isomorphous with the thiourea (Tu) complex $[Pd(Tu)_4]I_2$ [11]. The existence of the complex in the ionic form represents the high stability of $[Pt(Imt)_4]^{2+}$ ion.

The complex dications, $[Pd(Imt)_4]^{2+}$ and chloride anions are associated to each other through formation of hydrogen bonds. In the crystal packing of complexes, the molecules are H-bonded via N–H or C–H hydrogen atoms of Imt and Cl^- ions (Table 3). A view of the crystal packing of the complex showing hydrogen bonds is given in Fig. 2.

Table 1. Crystallographic data and structural refinement parameters for **I**

Parameter	Value
Empirical formula	$C_{12}H_{24}N_8S_4Cl_2Pd$
Formula Weight	585.93
Crystal system	Monoclinic
Space Group	*C*2/*c*
a, *b*, *c*, Å	17.5262(17), 8.04561(6), 16.2048(15)
α, β, γ, deg	90, 107.850(2), 90
V, Å^3	2174.9(3)
Z	4
ρ_{calcd}, g cm^{-3}	1.777
Temperature, K	296(2)
Crystal size, mm	0.40 × 0.34 × 0.22
F(000)	816
$\mu(MoK_\alpha)$, mm^{-1}	1.499
$\lambda(MoK_\alpha)$, Å	0.71073
2θ Range, deg	2.942–27.873
h, *k*, *l* limits	$-22 \le h \le 22$, $-10 \le k \le 9$, $-21 \le l \le 21$
Reflection collected/unique/R_{int}	9104/2589/0.0460
T_{min}/T_{max}	0.610/0.760
Data/restraints/parameters	2589/0/124
R_1, wR_2, S ($I > 2\sigma I$)	0.0420, 0.0818, 1.095
R_1, wR_2, S (all data)	0.0608, 0.0874, 1.1095
Largest diff. peak/hole, e Å^{-3}	0.703/–0.444

Table 2. A comparison of the selected geometrical data obtained using DFT calculations (in gas phase and DMSO solvent*) and from experiment for complex **I**

Bond	Theory	Experiment	Angle	Theory	Experiment
	d, Å			ω, deg	
Pd(1)–S(1)	2.476 (2.470)*	2.3362(10)	S(1)Pd(1)S(1)	180 (180)	180.0
Pd(1)–S(2)	2.477 (2.475)	2.3601(10)	S(1)Pd(1)S(2)	85.6 (88.1)	87.56(4)
C(1)–S(1)	1.776 (1.778)	1.710(4)	S(1)Pd(1)S(2)	94.4 (91.9)	92.44(4)
C(4)–S(2)	1.777 (1.764)	1.704(4)	S(2)Pd(1)S(2)	180 (180)	180.0
C(1)–N(1)	1.342 (1.350)	1.307(5)	C(1)S(1)Pd(1)	100.0 (101.7)	107.39(13)
C(1)–N(2)	1.333 (1.322)	1.331(5)	N(1)C(1)S(1)	125.3 (124.4)	127.4(3)
C(2)–N(1)	1.468 (1.475)	1.459(5)	N(2)C(1)S(1)	122.9 (124.4)	122.7(3)
C(2)–C(3)	1.553 (1.550)	1.532(6)	N(1)C(1)N(2)	111.8 (111.2)	109.9(3)
RMSD	0.075 (0.072)		RMSD	2.9 (2.4)	

* Values in parentheses represent the results obtained for DMSO solvent simulation.

In the IR spectrum of the complex shown in Fig. S1, the characteristic bands observed are (cm^{-1}): 498, 918 ν(C=S) and 1530 ν(C–N). For free Imt these bands were observed at 510, 925, and 1509 cm^{-1}, respectively. A low frequency shift in the ν(C=S) band and a high frequency shift in ν(C–N) band indicate the greater double bond character of the C–N bond on S-coordination of Imt to palladium(II) in the solid state. The ν(N–H) vibrations appeared at 3361 and 3125 cm^{-1}. A weak peak at 1608 cm^{-1} can be assigned

Table 3. Geometric parameters of hydrogen bond for **I**

Donor–H···Acceptor	Distance, Å			∠D–H···A, deg
	D–H	H···A	D···A	
N(1)–H(1)···Cl(1)	0.86	2.36	3.209(2)	149.6
N(1)–H(1)···S(2)	0.86	2.97	3.7494(18)	146.9
N(3)–H(3)···Cl(1)	0.86	2.46	3.180(4)	159.0
N(4)–H(4)···Cl(1)	0.86	2.36	3.463(4)	118.8
C(2)–H(2B)···Cl(1)	0.97	2.78	3.254(3)	153.7
C(3)–H(3A)···Cl(1)	0.97	2.84	3.199(3)	164.1
C(5)–H(5A)···Cl(1)	0.97	2. 94	3.895(5)	167.8

to NH_2 bending. The signals due to C–H stretching were observed at 2930 and 2889 cm^{-1}.

Infrared frequencies for the selected normal modes were also predicted theoretically (in gas phase and DMSO solvent) in this work in order to make the reliable assignment of the measured IR spectra. The theoretical assignment of the vibrational bands of Imt and complex **I** is displayed in Table 4. The IR frequencies predicted in the gas phase as well as in DMSO solvent are in good agreement. The biggest disparities concern with the ν(N–H) bands, which are calculated at 3526 and 3538 cm^{-1} in gas phase, whereas in the solvent case they are shifted towards higher wavenumbers (in the region of 3642–3675 cm^{-1}). The remaining vibrations are located in the similar range in both approaches, with differences no more than 24 cm^{-1}. The ν(Pd–S) vibration associated with the Pd–S bond formation is expected at low range of 264 and 244 cm^{-1} (in gas and DMSO respectively). At slightly higher frequency appears the ν(C=S) band (about 470 cm^{-1}). The region of 1360–1600 cm^{-1} is dominated by vibrations localized within the Imt ring: C–N stretching as well as C–H and N–H bending. The energetically superior are the ν(N–H) peaks, which are predicted at 3500–3700 cm^{-1}. With respect to the location of main vibrational bands in the theoretical and experimental spectra, it can be concluded that they match each other in decent accuracy, especially since any scaling factor was not applied in theoretical prediction of IR spectrum.

In ^{1}H NMR spectrum of the complex, the N–H signal of Imt was observed at a downfield position with respect to that in the free state (8.57 ppm vs. 7.98 ppm). The deshielding of N–H proton corresponds to an increase of the π electron density in the C–N bond upon complexation [18, 19, 40]. In ^{13}C NMR spectrum of **I** (Fig. S2), the appearance of CH_2 and >C=S resonances of Imt at 45.0 ppm and 178.2 ppm respectively, indicates its binding to palladium(II) (δ = 44.0 and 183.4 ppm respectively in the uncomplexed Imt). The upfield shift in the >C=S resonance is attributed to the lowering of >C=S bond order upon coordina-

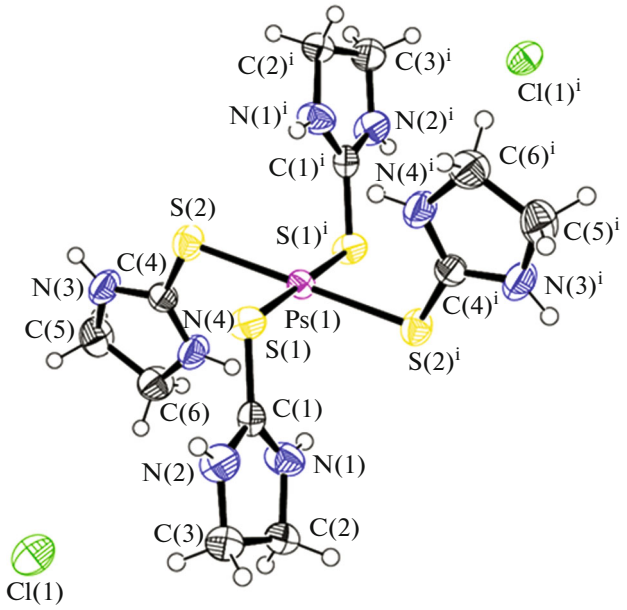

Fig. 1. Molecular structure of $[Pd(Imt)_4]Cl_2$ (**I**) (thermal ellipsoids at a 50% probability level).

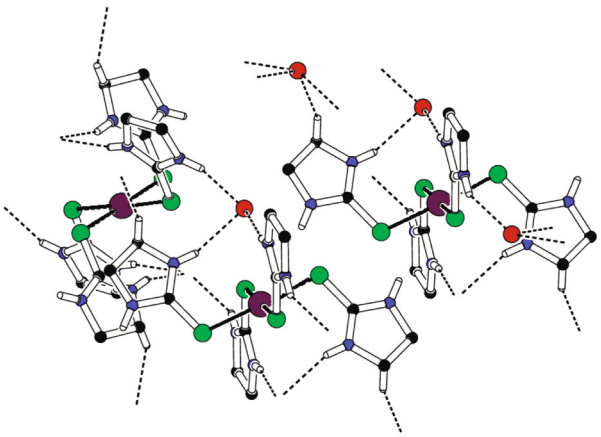

Fig. 2. The H-bonding pattern in complex **I**.

Table 4. Theoretically predicted IR absorption bands (cm^{-1}) for free ligand and its palladium(II) chloride complex. Data obtained in gas phase and using DMSO solvent simulation

Species	ν(C = S)	ν(N−H)	δ(NH)	ν(C−N)	δ(CH)	ν(Pd−S)
Imt	487 (464)*	3666, 3668 (3662, 3665)	1363 (1360)	1448 (1472)	1517, 1530 (1520, 1530)	
$[Pd(Imt)_4]Cl_2$	471, 475 (470)	3526, 3538 (3642, 3654, 3675)	1551, 1558 (1532, 1553)	1574, 1581 (1568, 1599)	1527 (1507, 1503)	264 (244)

* The results in parentheses were obtained using DMSO solvent simulation.

tion in agreement with the previous reports [17–20, 40–42]. The transfer of N → C(S) electron density produces a partial double bond character in the C–N bond, which causes a downfield shift (1 ppm) of CH_2 carbon atoms. The small shift shows that nitrogen atoms are not involved in coordination. The ^1H and ^{13}C NMR results are almost consistent with the earlier report [17].

The DFT optimized structures of complex $[Pd(Imt)_4]Cl_2$ (**I**) as well as three model complexes; $[Pd(Imt)_2Cl_2] \cdot 2$ Imt (**Ia**) and the related cyanide species, $[Pd(Imt)_2(CN)_2]_2$ (**II**) and $[Pd(Imt)_4][Pd(CN)_4]$ (**IIa**), are shown in Fig. S3. A comparison between the results of DFT optimization and X-ray structure determination made for complex **I** is displayed in Table 2. The data shows that the bond distances are overestimated in theoretical prediction, independent of the approach: gas phase or introducing DMSO solvent simulation. The root mean square error (RMSD) for both type of calculations is similar: 0.072–0.075 Å. The main source of this discrepancy is the estimation of Pd–S bond distance. It is larger by more than 0.1 Å in comparison with the experiment. Moreover, the Pd–S(1) and Pd–S(2) distances are nearly the same in theoretical study, while in experiment there is more significant divergence between them. In the case of bond angles, the difference between theory and experiment is 2.9° and 2.4° for the gas phase and DMSO solution, respectively. Unexpectedly, the DMSO solvent simulation does not improve much the DFT structure guess compared to the standard gas phase approach. It should be added that the geometrical parameters were overvalued also in the work of platinum(II) and palladium(II) thiourea chlorides that were predicted only in the gas phase therein [8]. Despite the fact of the numerical differences the theoretically obtained structures are in good agreement with crystal structure, including ligand orientation toward Pd atom and chlorine's positions.

In the non-ionic model specimen (**Ia**) Cl atoms occupy the first coordination sphere along with two sulfur atoms. A question then arises, which of these two structures (**I** or **Ia**) is more stable DFT calculations grant equivocal response. In Table 5 the electronic and Gibbs free energies (ΔG) are collected. Although in gas phase the **Ia** complex is more stable by −11.26 kcal/mol in terms of ΔG parameter, the DMSO results draw the altered picture. In such an environment, complex **I** is the more stable one (by 1.92 kcal/mol). It could be stated that the introduction of solvent into calculations made the model closer to the situation observed in crystal structure that results in complex **I** energetically more preferable. In the analogous cyanide complexes these observations repeat. The **IIa** form is more stable in gas phase calculations, while when the DMSO behavior is mimicked the more stable is the dimer (II) of mononuclear complex $[Pd(Imt)_2(CN)_2]$. This trend is present both in terms of electronic energies and ΔG, although in the case of Gibbs free energies less differences occur between two isomeric forms (by the ratio in range 2–4).

The NBO atomic charges calculated for optimized geometry of complex **I** are reported in Table S1. Differences between charges obtained in the gas phase and DMSO are insignificant (RMSD less than 0.035 e). The central palladium atom is positively charged (0.365 e in gas phase) and sulfur atoms connected with it withdraw the electron density gaining formal negative charge (about −0.2 e). In the case of Imt ring the nitrogen and carbon atoms are negatively and positively charged respectively, which is in line with their electronegativity. The charges on Cl atoms are −0.779e and −0.869e in gas phase and DMSO, respectively.

The HOMO and LUMO orbitals of complex **I** were indicated using DFT calculations. The visualization of these orbitals is portrayed in Fig. 3. According to the NBO analysis of canonical molecular orbitals, the HOMO orbital in the gas phase is localized only on Cl atoms (50% on the both lone pair orbitals of Cl, LP(Cl)), while LUMO is spread throughout the molecule (it is a mixture consisting of: 61% of the two σ*(Pd–S) orbitals and 39% of the two sulfur lone pair orbitals, LP(S)). The situation is comparable in DMSO solvent. HOMO orbital occupies two LP(Cl) and LUMO orbital, in turn is scattered again on the σ*(Pd–S) orbitals (divided evenly of 30%) and LP(S) ones (20% each).

Overall, in this study, the crystal structure of a palladium(II) complex of imidazolidine-2-thione, $[Pd(Imt)_4]Cl_2$ (**I**) is presented. Theoretical investigations of complex **I** and three related complexes; $[Pd(Imt)_2Cl_2]\cdot 2$Imt (**Ia**), $[Pd(Imt)_2(CN)_2]$ (**II**) and

Table 5. Electronic (E_{elec}, a.u.) and Gibbs free energies (ΔG, a.u. at 298 K) of the model complexes **I**, **Ia**, **II** and **IIa** studied in this work calculated at the B3LYP-D3/D95V(d,p)/LanL2DZ level of theory

System	E_{elec}	ΔG^{298}	ΔE_{elec}*	$\Delta(\Delta G)^{298}$**
I	−1107.225677 (−1107.280664)[b]	−1106.898763 (−1106.958639)	+9.26 (0.00)	+11.26 (0.00)
Ia	−1107.240443 (−1107.279471)	−1106.916711 (−1106.955572)	0.00 (+0.75)	0.00 (+1.92)
II	−1575.507322 (−1575.569867)	−1575.158251 (−1575.220599)	+19.78 (0.00)	+13.37 (0.00)
IIa	−1575.538841 (−1575.560870)	−1575.179561 (−1575.209672)	0.00 (+5.65)	0.00 (+6.86)

* Differences in relation to more stable complex (set as 0.00) expressed in kcal/mol.
** Results for DMSO solvent are given in parentheses.

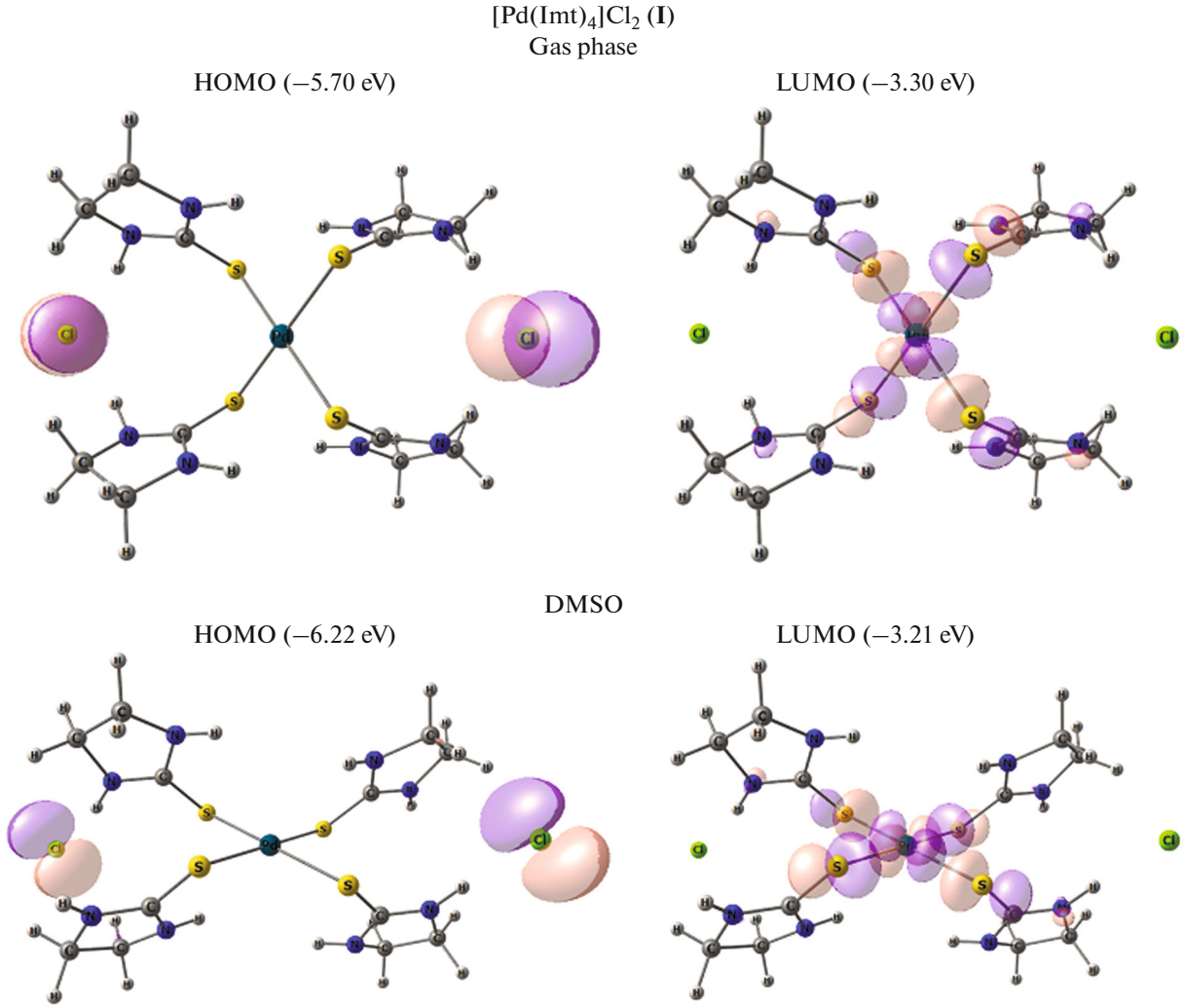

Fig. 3. The frontier molecular orbitals of complex **I** calculated at DFT level in gas phase and DMSO solvent (using 0.05 a.u. electron density isosurface).

$[Pd(Imt)_4][Pd(CN)_4]$ (**IIa**) were also carried out. The complex **I** exists in the ionic form in the solid state and the palladium atom in **I** adopts a square planar geometry. The structure is stabilized by H-bonding interactions. The DFT calculations predict that in DMSO the experimentally determined structure (**I**) is more stable in comparison to the corresponding nonionic structure, $[Pd(Imt)_2Cl_2]\cdot 2Imt$ (**Ia**), while in the gas phase **Ia** is the more stable structure. The same concerns with the energetic dependencies of **II** and **IIa** forms.

SUPPLEMENTARY MATERIALS

Supplementary materials are available for this article at DOI 10.1134/S107032842101005X and are accessible for authorized users.

REFERENCES

1. Garoufis, A., Hadjikakou, S.K., and Hadjiliadis, N., *Coord. Chem. Rev.*, 2009, vol. 253, p. 1384.
2. Moro, A.C., Mauro, A.E., Netto, A.V.G., et al., *Eur. J. Med. Chem.*, 2009, vol. 44, p. 4611.
3. Nadeem, S., Bolte, M., Ahmad, S., et al., *Inorg. Chim. Acta*, 2010, vol. 363, p. 261.
4. Zhang, L.-M., Li, H.-Y., Li, H.-X., et al., *Inorg. Chem.*, 2017, vol. 56, p. 11230.
5. Tyson, G.E., Tokmic, K., Oian, C.S., et al., *Dalton Trans.*, 2015, vol. 44, p. 14475.
6. Nadeem, S., Rauf, M.K., Ahmad, S., et al., *Transition Met. Chem.*, 2009, vol. 34, p. 197.
7. Nadeem, S., Rauf, M.K., Ebihara, M., et al., *Acta Crysrtallogr., Sect. E: Struct. Rep. Online*, 2008, vol. 64, p. m698.
8. Fuks, L., Sadlej-Sosnowska, N., Samochocka, K., and Starosta, W., *J. Mol. Struct.*, 2005, vol. 740, p. 229.
9. Jolley, J., Cross, W.I., Pritchard, R.G., et al., *Inorg. Chim. Acta*, 2001, vol. 315, p. 36.
10. Wang, Y.-L., Bi, W.-H., Li, X., and Cao, R., *Acta Crysrtallogr., Sect. E: Struct. Rep. Online*, 2004, vol. 60, p. m699.
11. De Munno, G., Gabriele, B., and Salerno, G., *Inorg. Chim. Acta*, 1995, vol. 234, p. 181.
12. Kahn, E.S., Rheingold, A.L., and Shupack, S.I., *J. Chem. Crystallogr.*, 1993, vol. 23, p. 697.
13. Butler, L.M., Creighton, J.R., Oughtred, R.E., and Raper, E.S., *Inorg. Chim. Acta*, 1983, vol. 75, p. 149.
14. Ahmad, S., Rüffer, T., Lang, H., et al., *Russ. J. Coord. Chem.*, 2010, vol. 36, p. 520. https://doi.org/10.1134/S1070328410070079
15. de Moura, T.R., Cavalcanti, S.L., de Godoy, P.R.D.V., et al., *Transition Met. Chem.*, 2017, vol. 42, p. 565.
16. Umakoshi, K., Ichimura, A., Kinoshita, I., and Ooi, S., *Inorg. Chem.*, 1990, vol. 29, p. 4005.
17. Tirmizi, S.A., Nadeem, S., Hameed, A., et al., *Spectroscopy*, 2009, vol. 23, p. 299.
18. Nadeem, S., Rauf, M.K., Bolte, M., et al., *Transition Met. Chem.*, 2010, vol. 35, p. 555.
19. Ahmad, S., Nadeem, S., Anwar, A., et al., J. *Mol. Struct.*, 2017, vol. 1141, p. 204.
20. Nadeem, S., Sirajuddin, M., Ahmad, S., et al., *Pharmaceut. Chem. J.*, 2017, vol. 51, p. 793.
21. Ahmad, S., Isab, A.A., and Perzanowski, H.P., *Can. J. Chem.*, 2002, vol. 80, p. 1279.
22. Isab, A.A., Al-Arfaj, A.R., Arab, M., and Hassan, M.M., *Transition Met. Chem.*, 1994, vol. 19, p. 87.
23. Sheldrick, G.M., *Acta Crystallogr., Sect. A: Found. Crystallogr.*, 2008, vol. 64, p. 112.
24. Sheldrick, G.M., Acta Crystallogr., *Sect. C: Struct. Chem.*, 2015, vol. 71, p. 3.
25. Spek, A.L., Acta Crystallogr., *Sect. D: Biol. Crystallogr.*, 2009, vol. 65, p. 148.
26. Becke, A.D., *J. Chem. Phys.*, 1993, vol. 98, p. 5648.
27. Lee, C., Yang, W., and Parr, R.G., *Phys. Rev., B,* 1988, vol. 37, p. 785.
28. Grimme, S., Antony, J., Ehrlich, S., and Krieg, H., *J. Chem. Phys.*, 2010, vol. 132, p. 154104.
29. Tomasi, J., Mennucci, B., and Cammi, R., *Chem. Rev.*, 2005, vol. 105, p. 2999.
30. Boys, S.F. and Bernardi, F., *Mol. Phys.*, 1970, vol. 19, p. 553.
31. Hay, P.J. and Wadt, W.R., *J. Chem. Phys.*, 1985, vol. 82, p. 299.
32. Dunning, T.H., Jr. and Hay, P.J., in *Modern Theoretical Chemistry*, Schaefer H.F. III, Ed., New York: Plenum, vol. 3, 1976.
33. Weinhold, F., Landis, C.R., and Glendening. E.D., *Inter. Rev. Phys. Chem.*, 2016, vol. 35, p. 399.
34. Frisch, M.J., Trucks, G.W., Schlegel, H.B., et al., Wallingford: Gaussian, Inc., 2016.
35. Orysyk, S.I., Bon, V.V., Zholob, O.A., et al., *Russ. J. Coord. Chem.*, 2014, vol. 40, p. 160. https://doi.org/10.1134/S1070328414030063
36. Burlov, A.S., Uraev, A.I., Lysenko, K.A., et al., *Russ. J. Inorg. Chem.*, 2015, vol. 60, p. 1481. https://doi.org/10.1134/S0036023615120062
37. Jomaa, M.Y., Altaf, M., Ahmad, S., et al., *Polyhedron*, 2018, vol. 141, p. 360.
38. Mahmood, R., Ahmad, S., Fettouhi, M., et al*., J. Mol. Struct.*, 2018, vol. 1156, p. 235.
39. Ahmad, S., Seerat-ur-Rehman, Arshad, M.N., et al., *Z. Naturforsch., B*, 2019, vol. 74, p. 565.
40. Isab, A.A., Fettouhi, M., Malik, M.R., et al., *Russ. J. Coord. Chem.*, 2011, vol. 37, p. 180. https://doi.org/10.1134/S1070328411030055
41. Mahmood, R., Sadaf, S., Is, A.A., et al., *Russ. J. Coord. Chem.*, 2012, vol. 38, p. 456. https://doi.org/10.1134/S1070328412060085
42. Ahmad, T., Mahmood, R., Lee, S.C., and Ahmad, S., *Russ. J. Coord. Chem.*, 2014, vol. 40, p. 125. https://doi.org/10.1134/S1070328414020018